Supporting Information

Boosting Type-I ROS Production of Molecular Photosensitizers Using Bridge-Assisted Superexchange Coupling

Lei Chen,[‡a] Shirong Yan,[‡a] Wu-Jie Guo,[a] Lu Qiao,[a] Xinyue Zhan,[a] Bin Liu,[*a] and Hui-Qing Peng[*a]

[a] State Key Laboratory of Chemical Resource Engineering, Beijing Advanced Innovation Center for Soft Matter Science and Engineering, Beijing University of Chemical Technology, No. 15, North Third Ring Road, Beijing 100029, China.

Materials and Methods

All the chemicals and reagents were purchased from commercial suppliers and used without further purification. The organic solvents are analytically pure. ^{1}H NMR and ^{13}C NMR spectra were measured on a Bruker Advance III (400 MHz) spectrometer. High-resolution mass spectrometry (HRMS) measurements were performed on a Waters UPLC/Premier mass spectrometer. UV-vis absorption spectra were determined by a SHIMADZU UV-2600i spectrophotometer. The photoluminescence spectra were measured by a SHIMADZU RF-6000 spectra fluorophotometer. Phosphorescence and lifetime of delayed emission spectra were recorded on an Agilent. Cary Eclipse spectrophotometer. Absolute fluorescence quantum yields were measured at room temperature by using a FLS1000 Edinburgh spectrometer and an integrated sphere. ROS assays were conducted by using a Xenon lamp (Microsolar300, Beijing Perfectlight). EPR analysis was performed on a Bruker E500 spectrometer. X-ray photoelectron spectroscopy (XPS) valence band spectrum was obtained by the Thermo Scientific K-Alpha instrument. Mott-Schottky analysis was carried out with CHI760E electrochemical workstation. Dynamic light scattering (DLS) investigations were carried out with a Malvern Zetasizer Nano ZS90 (Malvern Instruments, UK). Transmission electron microscopy (TEM) images were obtained using a Hitachi HT7700 instrument. The cell viability was detected by a CCK-8 kit, and the absorbance of each sample was measured at 450 nm using a microplate reader (PerkinElmer Victor3t). CLSM images were collected on a confocal laser scanning microscope (STELLARIS 5). Flow cytometry was carried out with CytoFLEX (Beckman Coulter).

Preparation of nanoparticles (NPs). COCN NPs and **CNCN NPs** were prepared by using nanoprecipitation method. In detail, **COCN** or **CNCN** (1 mg) and Pluronic F127 (10 mg) were dissolved in 1 mL of tetrahydrofuran (THF), respectively. The obtained solution was then mixed homogeneously via ultrasound for 10 min and then injected into deionized water (9 mL) with continuous stirring. The remaining THF was removed with a rotary evaporator.

Detection of ROS production. DCFH was used as an indicator for the detection of ROS in the solution. When ROS is generated in the system, the non-fluorescent DCFH will be oxidized and emit obvious fluorescence at 525 nm. Compounds (5 μM) were dissolved in 2 mL water containing 1 μM of DCFH. The mixture was then placed in a cuvette and irradiated under white light (35 mW·cm^{-2}) irradiation. The fluorescence intensity change of the sample at 525 nm was recorded by the fluorescence spectrometer.

Detection of $^1O_2$ production. ABDA was used as an indicator to evaluate $^1O_2$ generation of compound in solution under white light irradiation. Compounds (5 μM) were dissolved in 2 mL water containing 100 μM of ABDA. The mixture was irradiated under white light (35 mW·cm^{-2}) irradiation. The absorbance decrease of ABDA at 378 nm was recorded at various irradiation time.

Detection of $O_2^{-\bullet}$ production. DHR123 was used as an indicator for the detection of $O_2^{-\bullet}$ in solution. When $O_2^{-\bullet}$ is generated in the system, the DHR 123 will be oxidized and emit strong fluorescence centered at 526 nm. Compounds (5 μM) were dissolved in 2 mL water containing 10 μM of DHR 123. The mixture was irradiated under white light (35 mW·cm^{-2}) irradiation. The fluorescence change of the sample at 526 nm was recorded by the fluorescence spectrometer. DHE was also used as an indicator for the detection of $O_2^{-\bullet}$ in solution. When $O_2^{-\bullet}$ is generated in the system, DHE can be oxidized to form ethidium which intercalates into RNA and emits bright fluorescence at 580 nm. **COCN NPs** or **CNCN NPs** (5 μM) were dissolved in 2 mL PBS containing 40 μM of DHE and 500 μg/mL RNA. The mixture was irradiated under white light (35 mW·cm^{-2}) irradiation. The fluorescence change of the sample at 580 nm was recorded by the fluorescence spectrometer.

Detection of •OH production. HPF was used as an indicator for the detection of •OH in solution. When •OH is generated in the system, the HPF will be oxidized and emit strong fluorescence centered at 515 nm. Compounds (5 μM) were dissolved in 2 mL water containing 10 μM of HPF. The mixture was irradiated under white light (35 mW·cm^{-2}) irradiation. The fluorescence change of the sample at 515 nm was recorded by the fluorescence spectrometer.

Electron paramagnetic resonance (EPR) Measurement. EPR measurement was used to identify the type of ROS using 2,2,6,6-tetramethylpiperidine (TEMP) as the $^1O_2$ indicator and 5,5-dimethyl-1-pyrroline-N-oxide (DMPO) as the radical indicator. For $^1O_2$ and $O_2^{-\bullet}$ detection, samples were prepared by mixing 200 μL, 500 μM of compounds and 10 μL TEMP or 0.2 M DMPO in DMF, respectively. For •OH detection, samples were prepared by mixing 200 μL, 500 μM of compounds and 0.2 M DMPO in water. EPR signals were recorded by adding samples through a capillary tube under white light (35 mW·cm^{-2}) irradiation for 2 min.

Theoretical Calculations. The ground-state geometries were optimized using B3LYP density function theory (DFT) at the basis set level of 6-311G (d). The excited-state geometries in water were optimized using the time-dependent density function theory (TD-DFT) method, with M06-2X hybrid functional at the basis set level of 6-311G (d), performed using Gaussian 09, supported by High performance computing platform of BUCT. Single-point energy calculations were carried out in all cases.

Nelsen's four-point method were performed in water phase, modeled by the polarizable continuum model (PCM).[1, 2] Vertical electronic transitions were obtained using non equilibrium solvation and performed via a two-steps job: first, a single point energy calculation was performed on the initial state, specifying noneq=write in the PCM input section to store the information about non-equilibrium solvation based on the initial state. Second, the actual state specific calculation is performed reading the non-equilibrium solvation information, using noneq=read, and specifying the checkpoint file from the first step. The transitions of the optimized states were analyzed based on the natural transition orbitals. The electron and hole analysis and interfragment charge transfer analysis were performed with Multiwfn 3.7. The spin-orbit coupling (SOC) values were calculated by OCRA.

XPS analysis. The valence band (VB) potential of **COCN** can be calculated using eq (1), where E_{NHE} is the VB potential of **COCN** versus the normal hydrogen electrode (NHE); E_F is the VB potential below the Fermi level (E_F); Φ is the work function. The XPS valence band spectrum of **COCN** show that the E_F is 3.08 V (Fig. 2f). The work function (Φ) is 4.20 eV. The calculated VB potential of **COCN** is 2.84 V versus NHE.

$$E_{NHE} = E_F + \Phi - 4.44 \quad (1)$$

Mott-Schottky analysis. Mott-Schottky analysis was conducted a by using the three-electrode system. A carbon paper electrode attached **COCN** was used as the working electrode, the platinum electrode and the Hg/Hg_2Cl_2 electrode were used as the counter electrode and reference electrode, respectively. The measurement was conducted in 0.1 M sodium sulfate solution.

Cell viability. 4T1 cells were previously plated in 96-well plates. Then, the cells were incubated with DMEM containing 10% (v/v) Fetal Bovine Serum (FBS), 0.5, 1, 2, 4, 6, 8, 10, and 16 μM **COCN NPs** at 37 °C for 4 h, respectively. Subsequently, the samples were irradiated with or without white light (35 mW·cm^{-2}) for 15 min. Afterwards, the abundant materials were placed with a fresh medium and the samples were incubated at 37 °C for 24 h. The cell viability was detected by CCK-8 according to the proposal and the results was analyzed by a microplate reader.

Cell Culture and Imaging. 4T1 cells were cultured in DMEM (high glucose) supplemented with 10% (v/v) FBS at 37 °C, 5% CO_2. 4T1 cells were plated in a 35 mm glass bottom confocal dish in advance. Then, the cells were incubated with 5 μM **COCN NPs** or **CNCN NPs** at 37 °C for 1, 2, 4, and 6 h. After washing abundant materials and dyes with PBS, the samples were captured by a confocal microscope.

Confocal colocalization. For co-staining with Lyso-tracker Green, cells were first incubated with compound and Lyso-tracker Green at 37 °C for 30 min. The medium was then removed and the cells were

rinsed with PBS for three times and then imaged under the confocal microscope. For **COCN NPs**, the emission filter was 560-600 nm; for Lyso-tracker Green, the excitation was 488 nm and the emission filter was 500-550 nm.

Calcein-AM/PI staining of 4T1 cells in PDT experiments. The 4T1 cells were seeded on 35 mm confocal dishes and incubated for 24 h. The medium was then replaced with a fresh culture medium containing of **COCN NPs** (8 μM) and incubated for 4 h. After that, the cells were irradiated with white light (35 mW·cm^{-2}) for 15 min. The cells were further cultured for 6 h, and the culture medium was replaced with DMEM containing 5 μM calcein-AM and 5 μM propidium iodide (PI). After further incubation for 20 minutes, the calcein-AM and PI solution was removed and washed three times with PBS buffer. Fluorescence images of calcein-AM and PI staining the cells were immediately captured by microscopy.

Flow Cytometry Test of Apoptosis. The 4T1 cells were seeded on 6 well cell culture plates and incubated for 24 h. The medium was then replaced with fresh culture medium containing **COCN NPs** (8 μM) and incubated for 4 h. Then, the cells were irradiated with white light (35 mW·cm^{-2}) for 15 min. After further incubation, the cells were collected and treated with AnnexinV-FITC/PI cell apoptosis detection kit. Flow cytometry was used to detect cell apoptosis.

Synthesis and Characterization

Synthesis of COCO. Piperazine (1.7 g, 20 mmol), (4-fluorophenyl)-(4-methoxyphenyl)methanone (9.2 g, 40 mmol), and potassium carbonate (5.52 g, 40 mmol) were added into 200 mL dimethyl sulfoxide (DMSO) in a flask and the mixture was refluxed at 140 °C for 12 h. After cooling to room temperature, 300 mL water was added to the mixture to induce the formation of a precipitate, and then the mixture was filtered to obtain a yellow solid. The yellow solid was recrystallized with dichloromethane (DCM) and petroleum ether (PE) to obtain the product. Yield: 8.5 g (84.0%). ^{1}H NMR (400 MHz, DMSO-d_6) δ 7.67 (t, J = 8.2 Hz, 8H), 7.07 (d, J = 8.5 Hz, 8H), 3.85 (s, 6H), 3.56 (s, 8H). ^{13}C NMR (101 MHz, Chloroform-d) δ 162.60, 153.24, 132.39, 132.25, 132.19, 132.07, 131.14, 128.41, 118.52, 113.62, 113.47, 113.40, 55.46, 47.22. MS: m/z [M+H]$^+$ calculated for $C_{32}H_{30}N_2O_4$, 507.2239; found, 507.2251.

Synthesis of COCN. **COCO** (1.12 g, 2 mmol), malononitrile (0.2 g, 3 mmol), and 40 mL DCM were placed into a flask and cooled in an ice bath. Titanium tetrachloride (TiCl$_4$, 2 mL) was slowly added and the mixture was stirred for 30 min at 0 °C. After reaching room temperature, 2 mL of piperidine was

added to the mixture, which was then stirred for 12 h at 90 °C. The organic phase was extracted with ethyl acetate (EA). The product was purified by silica gel column chromatography using PE/EA (3/1, v/v) as the eluting agent to obtain **COCN** as a yellow solid. Yield: 0.65 g (58.7%). ^{1}H NMR (400 MHz, DMSO-d_6) δ 7.66 (t, J = 8.1 Hz, 4H), 7.40 (dd, J = 23.9, 9.0 Hz, 4H), 7.14-7.01 (m, 8H), 3.86 (d, J = 5.1 Hz, 6H), 3.59 (d, J = 29.2 Hz, 8H). ^{13}C NMR (101 MHz, DMSO-d_6) δ 193.13, 173.33, 163.10, 162.60, 153.73, 153.38, 133.68, 133.43, 132.22, 131.99, 131.12, 128.85, 126.95, 124.10, 116.62, 116.44, 114.64, 114.10, 113.33, 113.23, 73.24, 56.08, 55.93, 46.39, 46.02. MS: m/z [M+H]$^+$ calculated for $C_{35}H_{30}N_4O_3$, 555.2351; found, 555.2376.

Synthesis of CNCN. **COCO** (1.12 g, 2 mmol), malononitrile (0.79 g, 12 mmol), and 40 mL DCM were added to a flask and cooled in an ice bath. TiCl$_4$ (2 mL) was then added slowly and the mixture was stirred for 30 min at 0 °C. After reaching room temperature, 2 mL of piperidine was added, which was then stirred for 12 h at 90 °C. The organic phase was extracted with EA. The product was purified by silica gel column chromatography using PE/EA (3/1, v/v) as the eluting agent to obtain **CNCN** as a yellow solid. Yield: 0.52 g (43.2%). ^{1}H NMR (400 MHz, Chloroform-d) δ 7.86-7.77 (m, 4H), 7.49-7.41 (m, 4H), 7.04-6.89 (m, 8H), 3.91 (s, 6H), 3.68-3.55 (m, 8H). ^{13}C NMR (101 MHz, DMSO-d_6) δ 173.34, 163.09, 153.59, 133.68, 133.42, 128.84, 124.01, 116.62, 116.44, 114.63, 113.07, 73.15, 60.23, 56.08, 55.37, 45.82. MS: m/z [M+H]$^+$ calculated for $C_{38}H_{30}N_6O_2$, 603.2464; found, 603.2499.
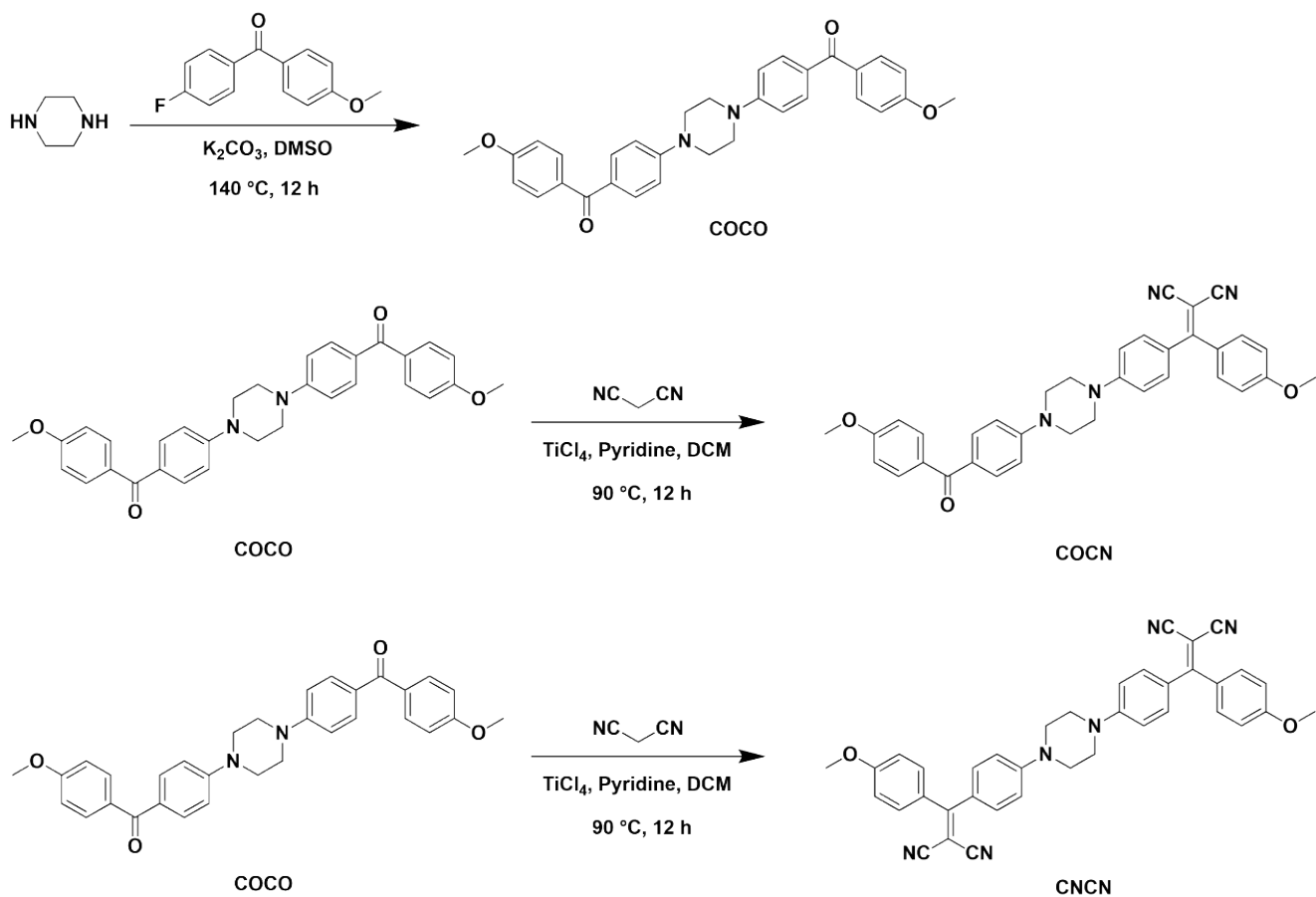
Scheme S1. Synthetic route of **COCO**, **COCN**, and **CNCN**.
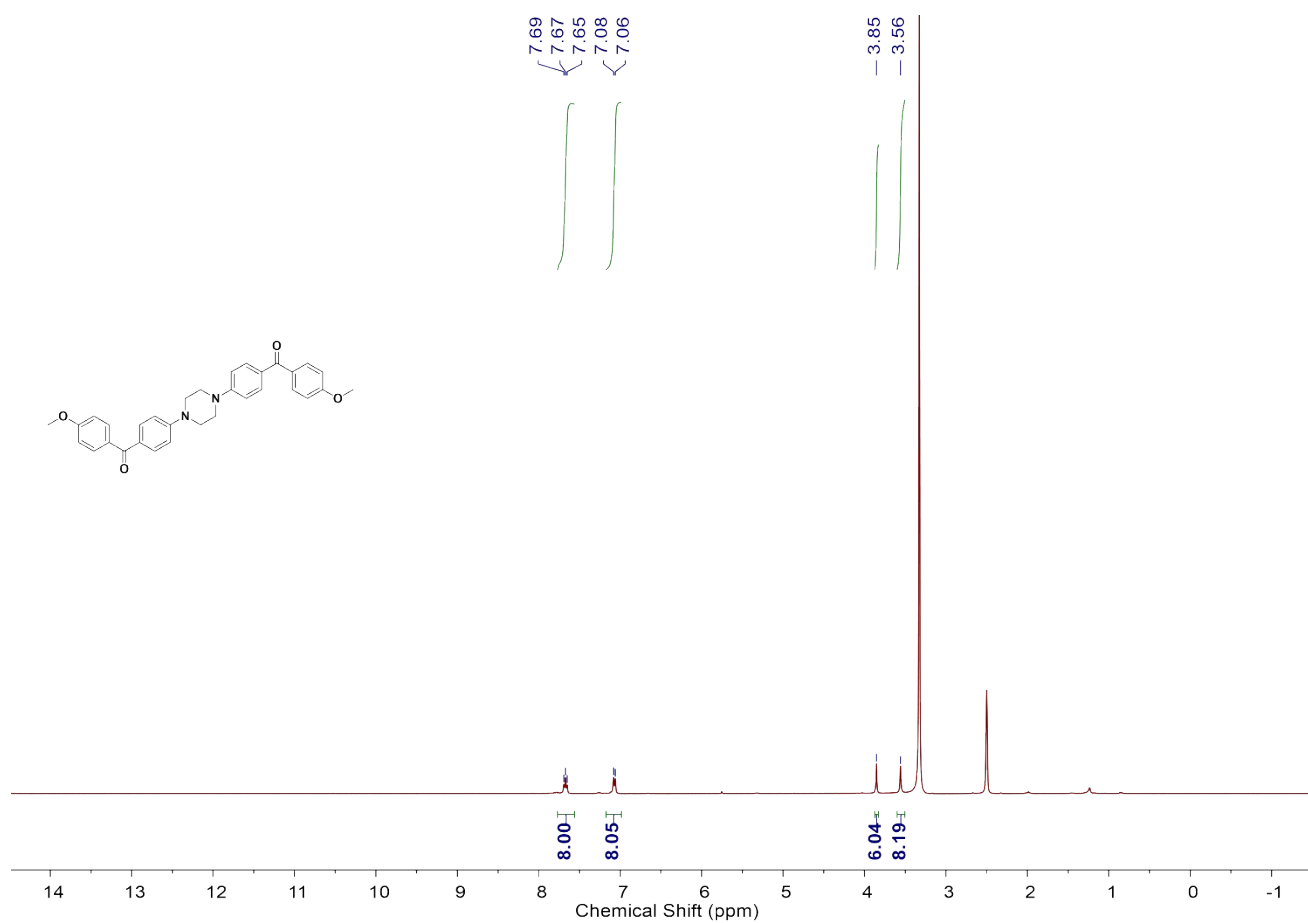
Figure S1. ^{1}H NMR spectrum of **COCO** in DMSO-d_6.
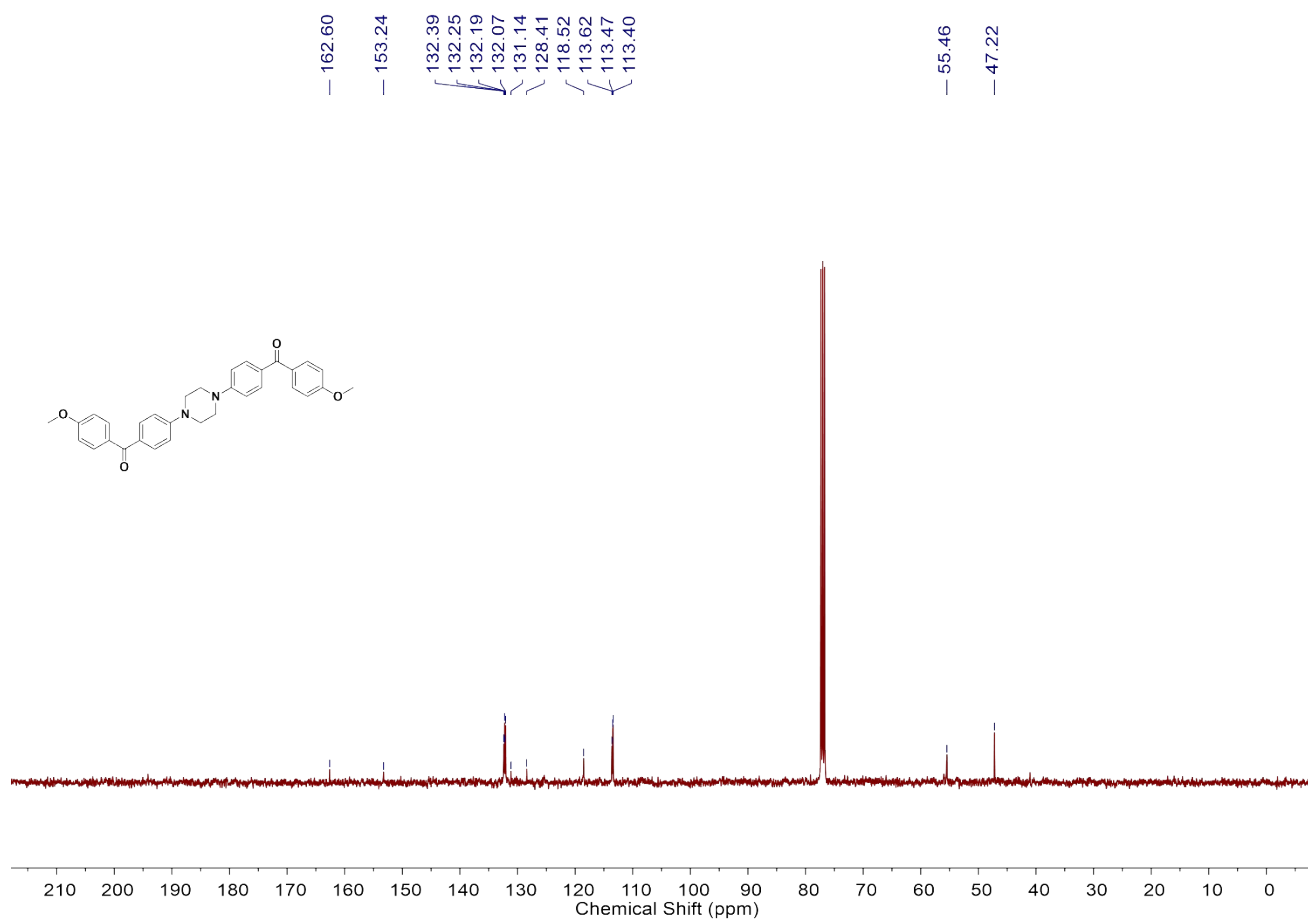
Figure S2. ^{13}C NMR spectrum of **COCO** in Chloroform-*d*.
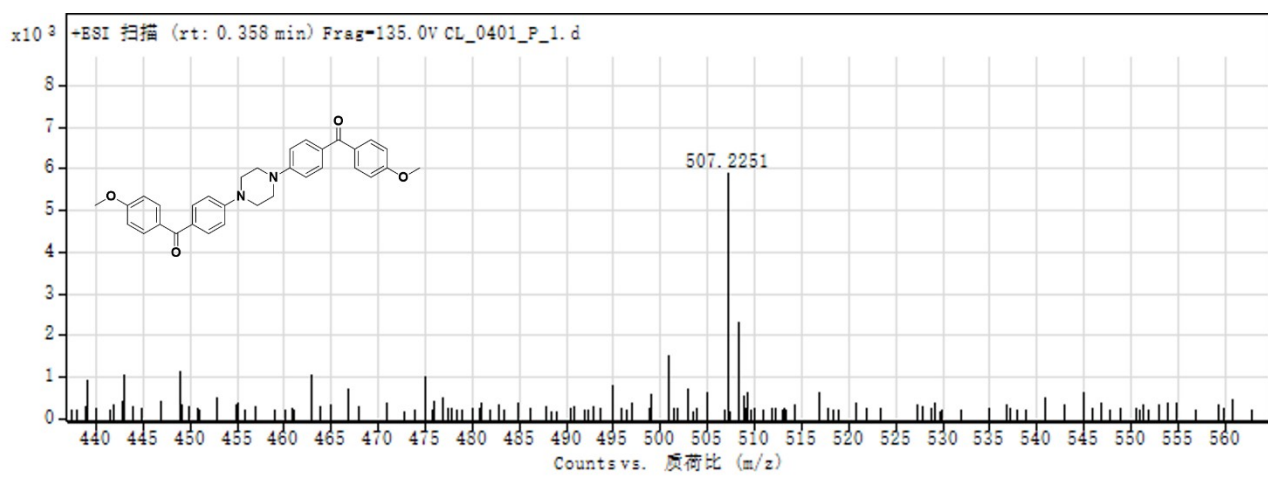
Figure S3. HRMS spectrum of **COCO** in DMSO.
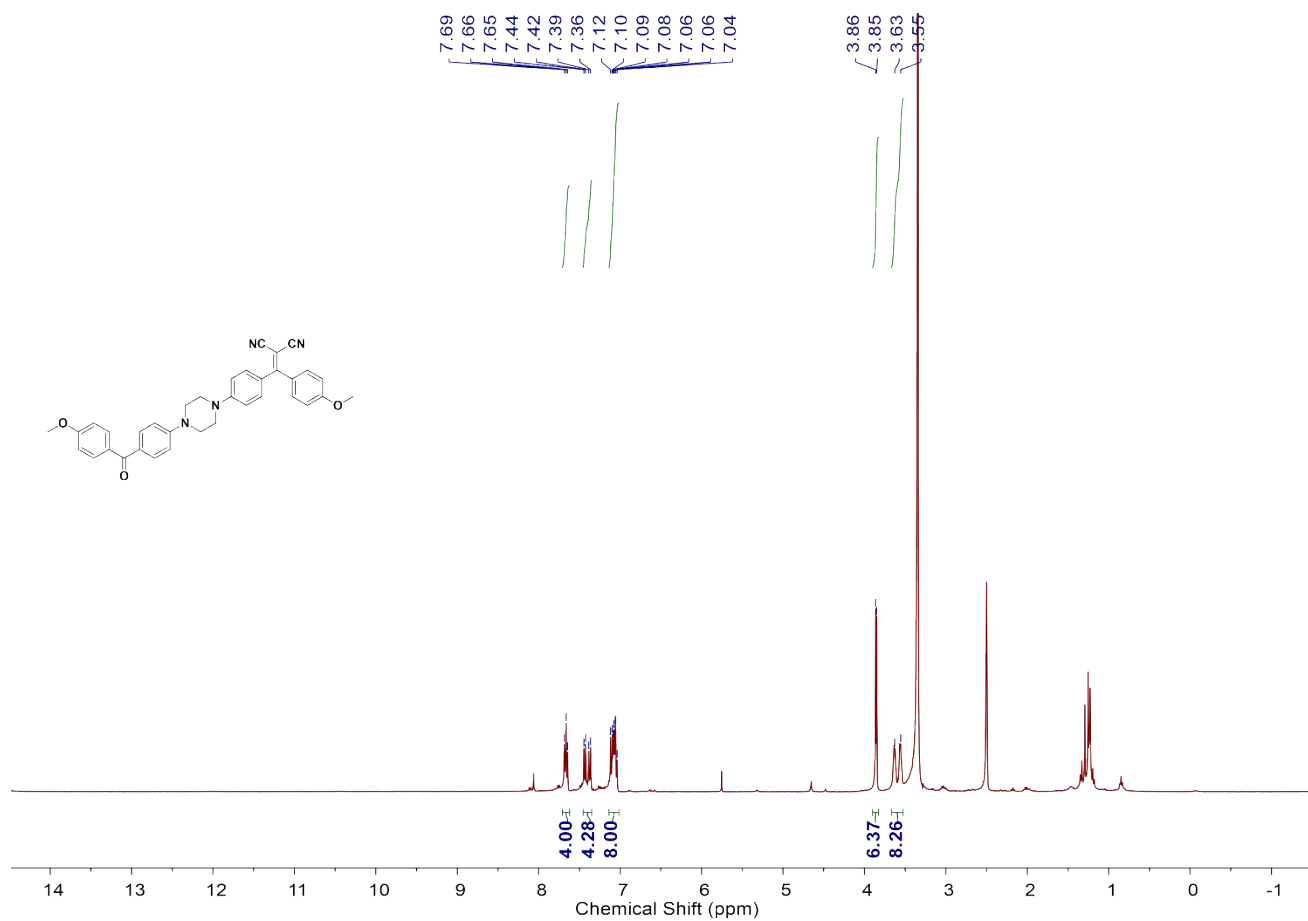
Figure S4. ^{1}H NMR spectrum of **COCN** in DMSO-d_6.
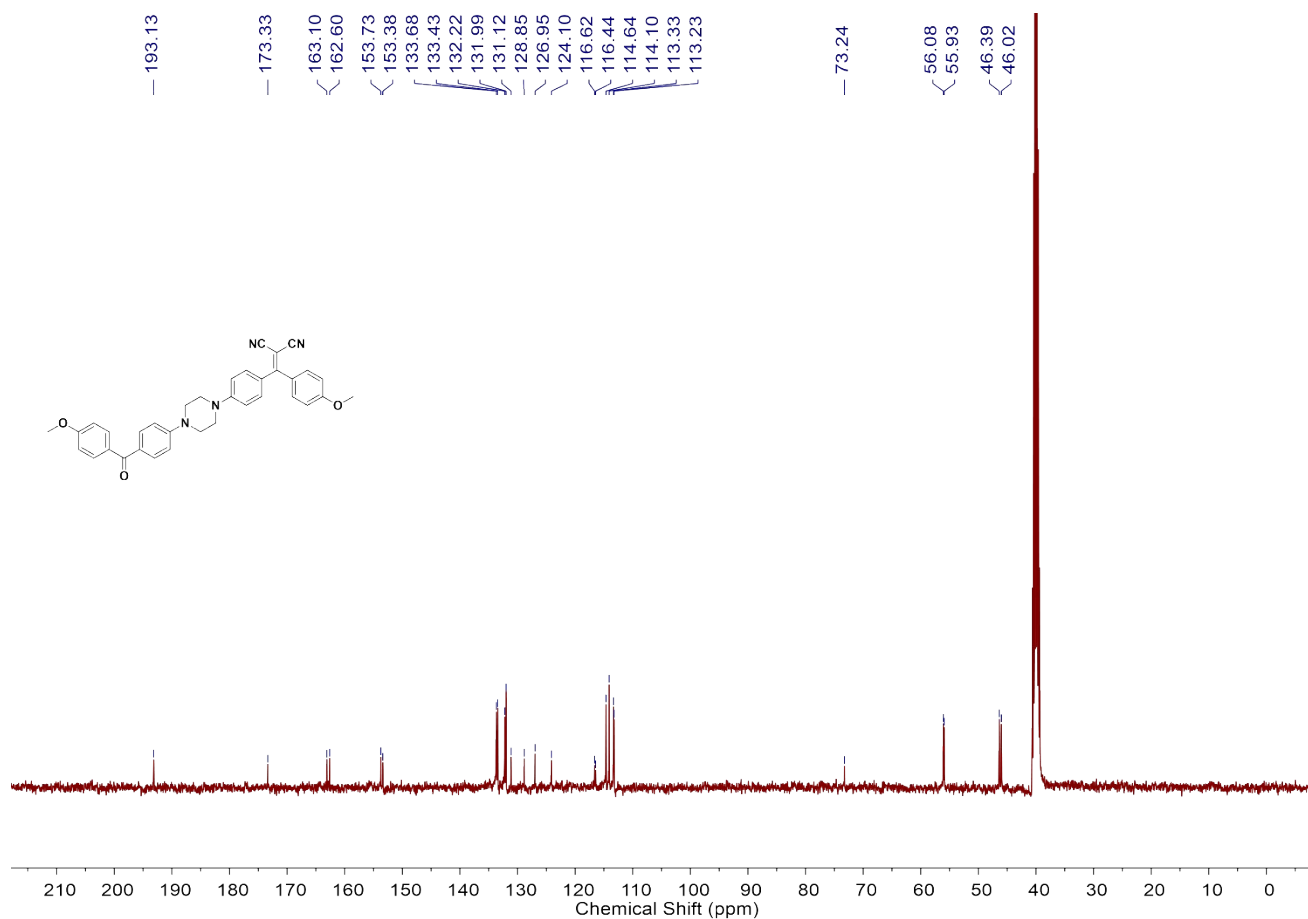
Figure S5. ^{13}C NMR spectrum of **COCN** in DMSO-d_6.
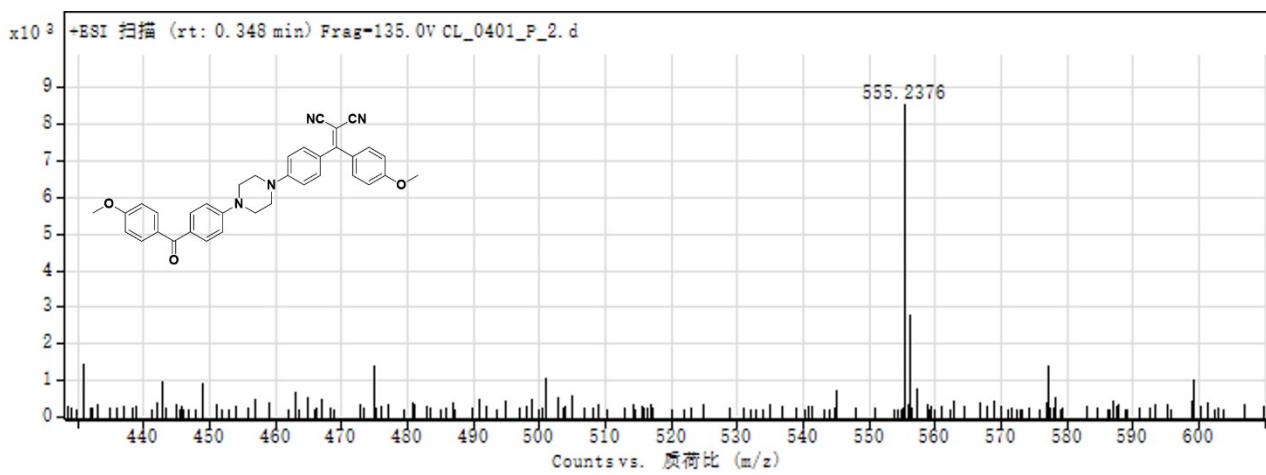
Figure S6. HRMS spectrum of **COCN** in DMSO.
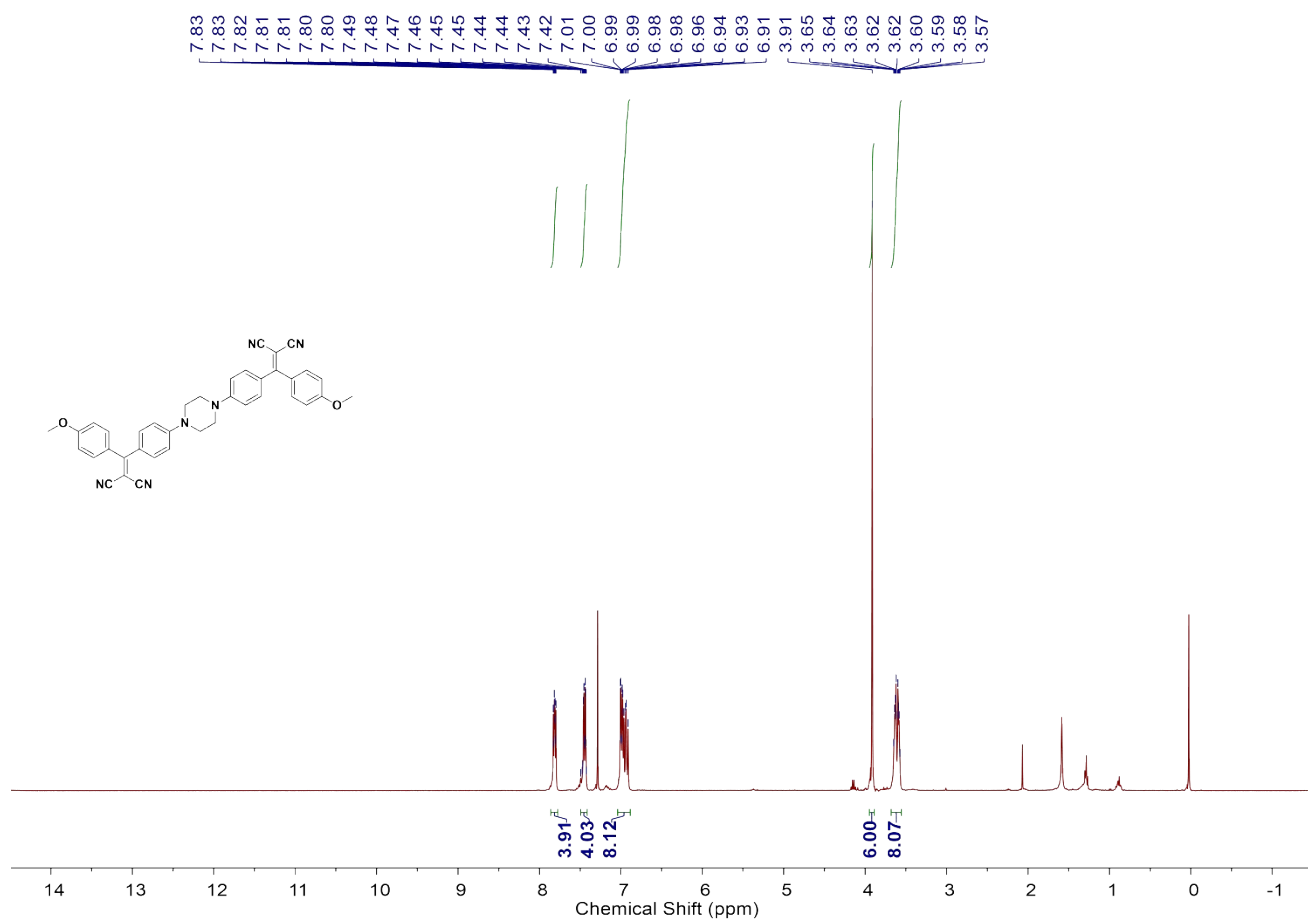
Figure S7. ^{1}H NMR spectrum of **CNCN** in Chloroform-*d*.
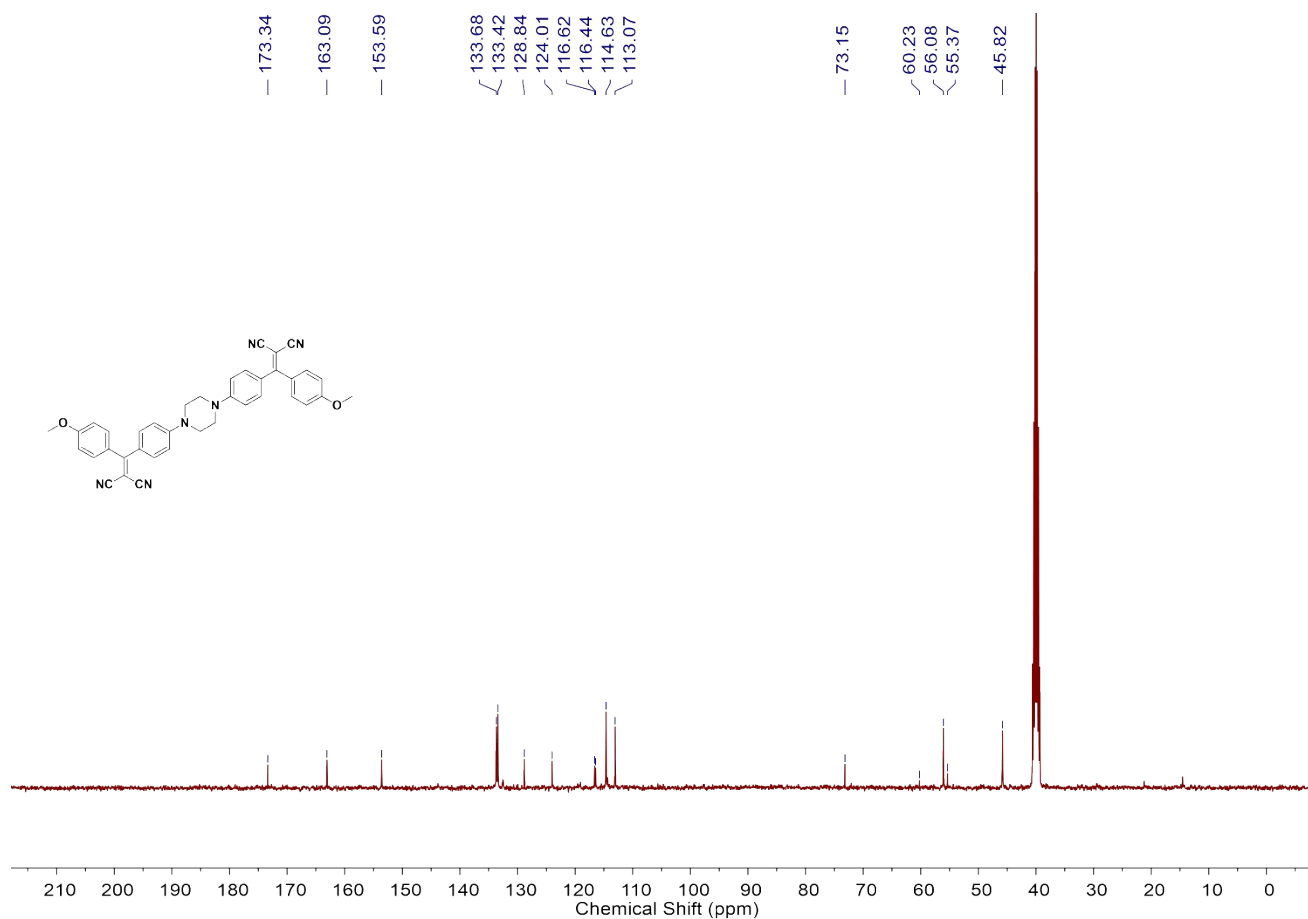
Figure S8. ^{13}C NMR spectrum of **CNCN** in DMSO-d_6.
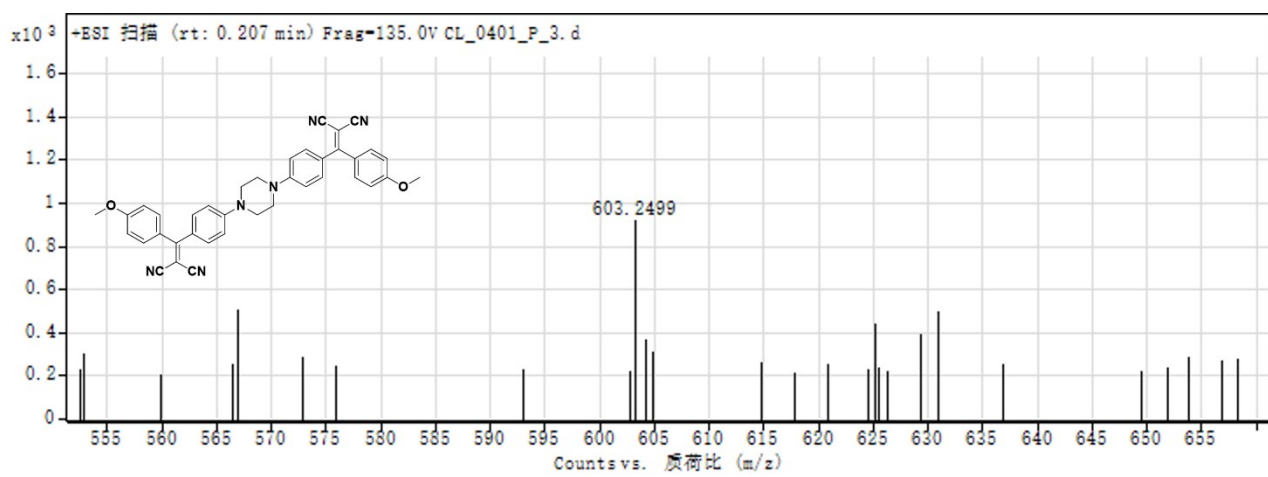
Figure S9. HRMS spectrum of **CNCN** in DMSO.
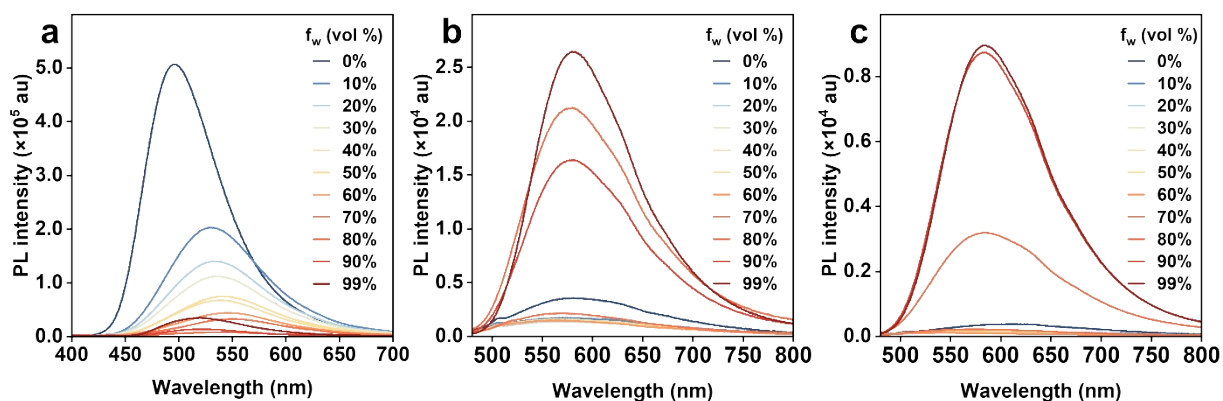
Figure S10. PL curves of (a) **COCO**, (b) **COCN**, and (c) **CNCN** in THF/H_2O mixtures with different H_2O fractions (f_w) (**COCO**, **COCN**, or **CNCN**: 10 μM).
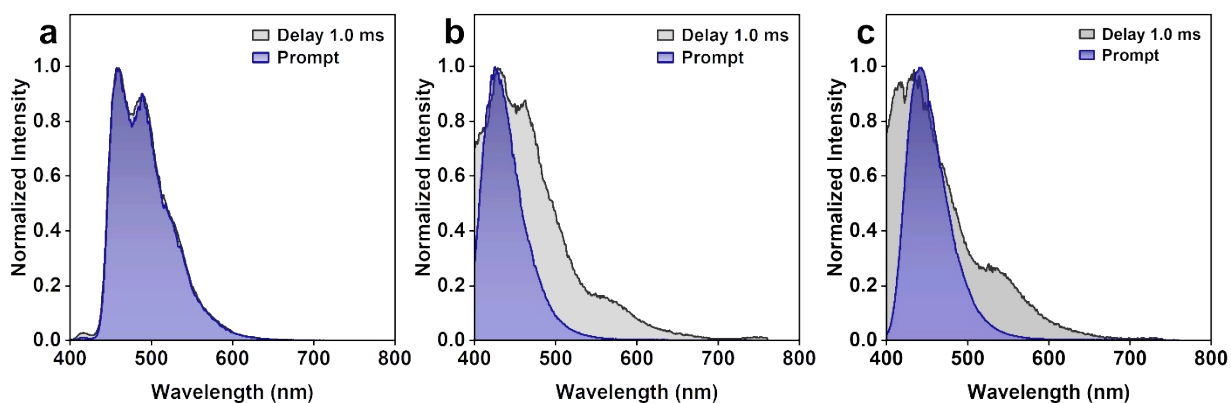
Figure S11. Steady and delayed emission spectra of (a) **COCO**, (b) **COCN**, and (c) **CNCN** at 77 K.
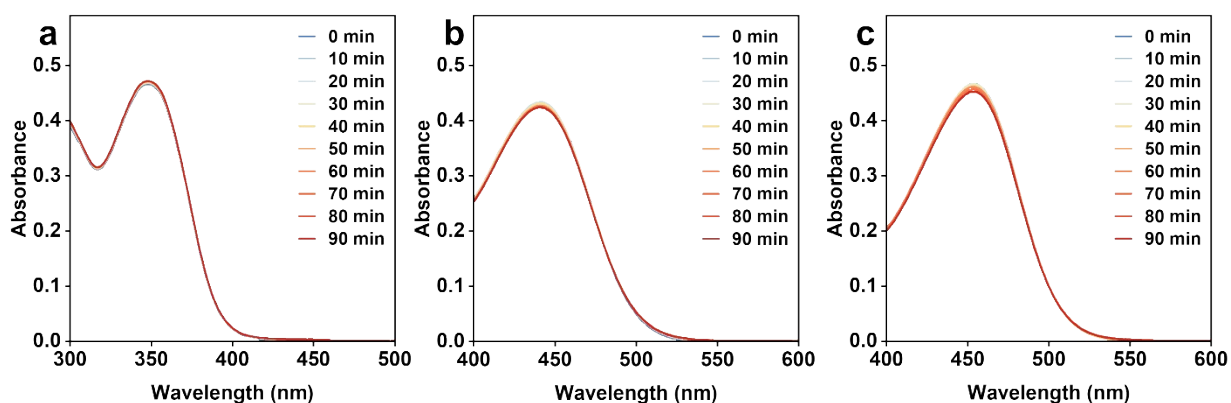
Figure S12. Absorption spectra of (a) **COCO**, (b) **COCN**, and (c) **CNCN** in DMSO solution under white light (35 mW·cm^{-2}) irradiation for 90 min (**COCO, COCN**, or **CNCN**: 25 μM).
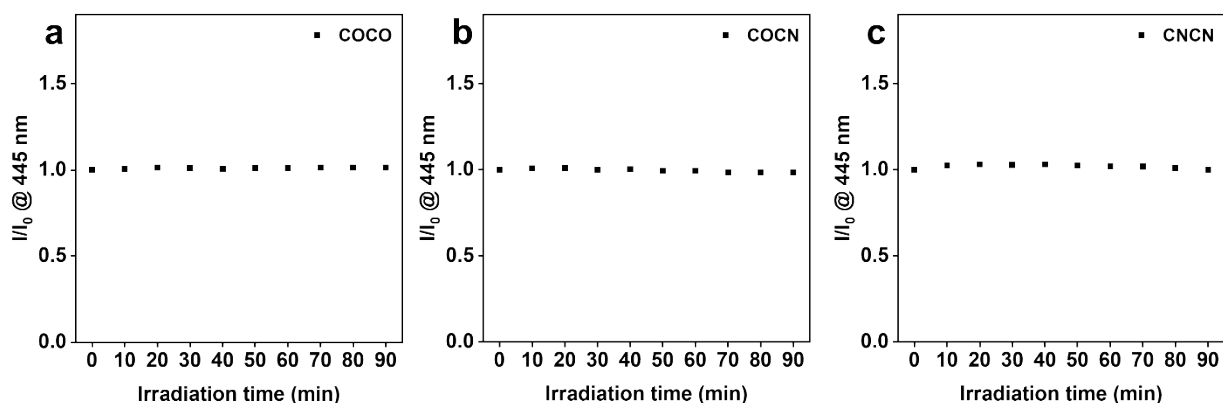
Figure S13. Absorbance decay of (a) **COCO**, (b) **COCN**, and (c) **CNCN** in DMSO solution under white light (35 mW·cm^{-2}) irradiation for 90 min (**COCO**, **COCN**, or **CNCN**: 25 μM).
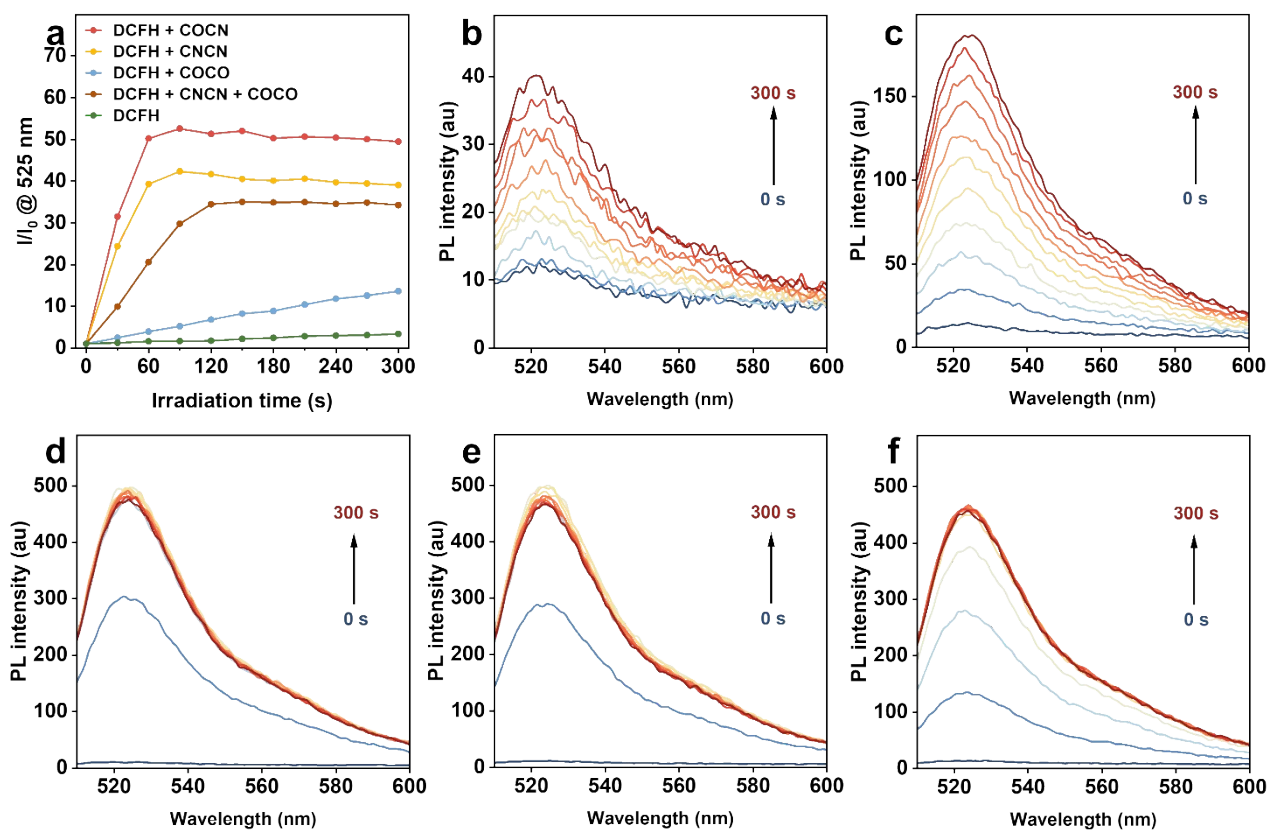
Figure S14. (a) ROS generation by the three compounds upon white light (35 mW·cm^{-2}) irradiation using DCFH as an indicator. PL spectra of DCFH solutions in the presence of (b) blank, (c) **COCO** (5 μM), (d) **COCN** (5 μM), (e) **CNCN** (5 μM), and (f) **COCO** (2.5 μM) with **CNCN** (2.5 μM) under white light (35 mW·cm^{-2}) irradiation for different times (DCFH: 1 μM).
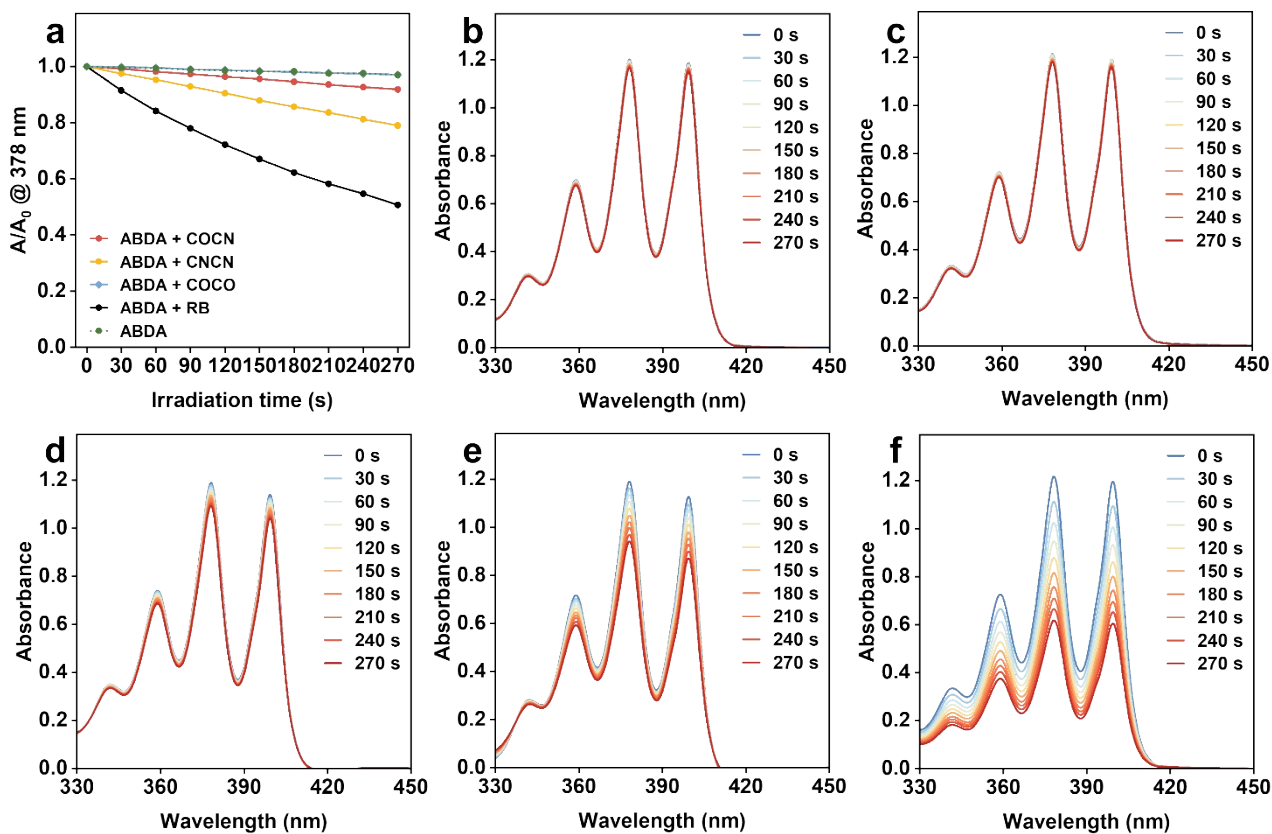
Figure S15. (a) Absorbance decay of ABDA in the presence of **COCO**, **COCN**, **CNCN**, or RB under white light irradiation. Absorption spectra of ABDA solutions in the presence of (b) blank, (c) **COCO**, (d) **COCN**, (e) **CNCN**, and (f) RB under white light (35 mW·cm^{-2}) irradiation for different times (ABDA: 100 μM; **COCO**, **COCN**, **CNCN**, or RB: 5 μM).
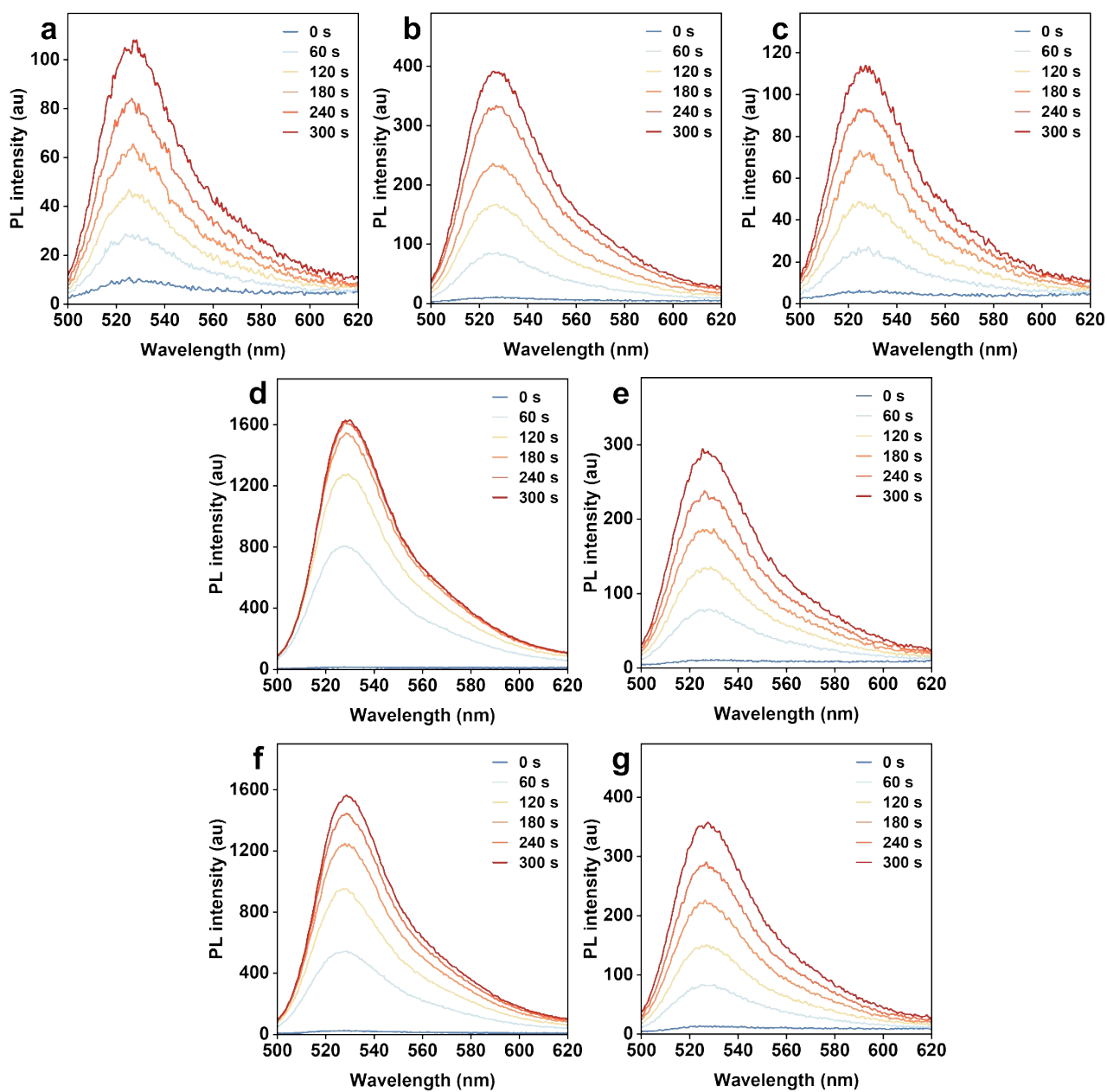
Figure S16. PL spectra of DHR123 solutions in the presence of (a) blank, (b) **COCO**, (c) **COCO** with Vc, (d) **COCN**, (e) **COCN** with Vc, (f) **CNCN**, and (g) **CNCN** with Vc under white light (35 mW·cm^{-2}) irradiation for different times (DHR123: 10 μM; Vc: 100 μM; **COCO**, **COCN**, or **CNCN**: 5 μM).
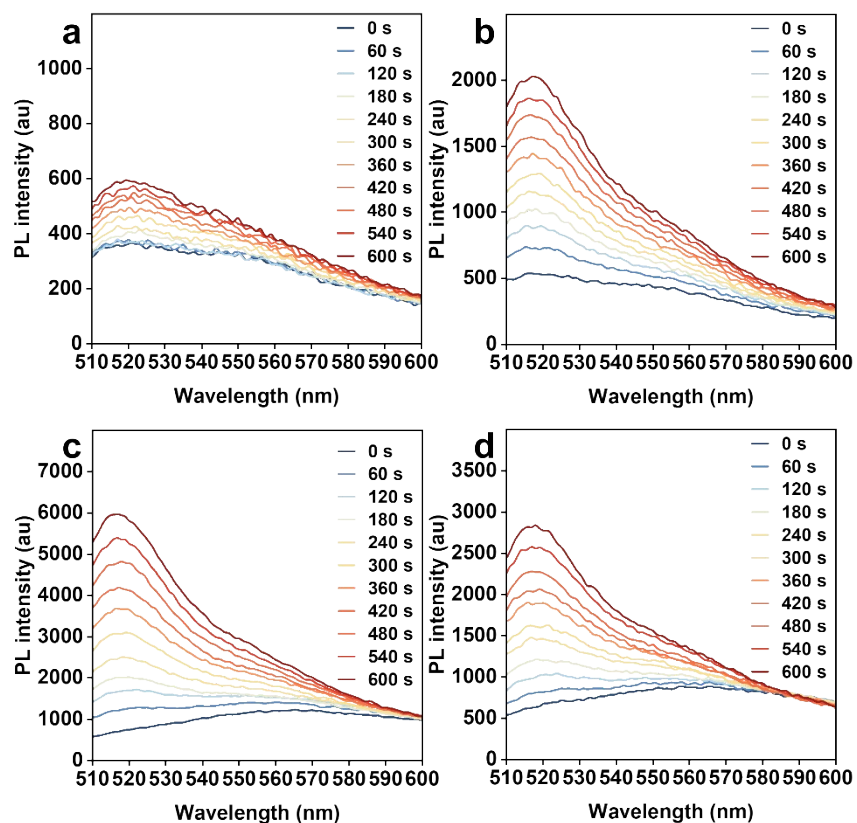
Figure S17. PL spectra of HPF solutions in the presence of (a) blank, (b) **COCO**, (c) **COCN**, and (d) **CNCN** with white light (35 mW·cm^{-2}) irradiation for different times (HPF: 10 μM; **COCO**, **COCN**, or **CNCN**: 5 μM).
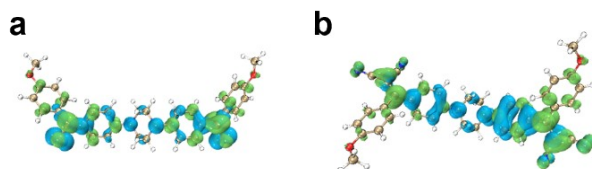
Figure S18. Hole-electron distributions of (a) **COCO** and (b) **CNCN** at S$_1$ excited state.

LUMO
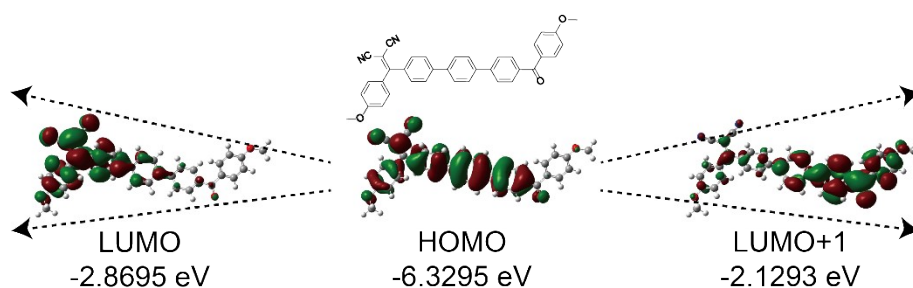-2.8695 eV

HOMO
-6.3295 eV

LUMO+1
-2.1293 eV

Figure S19. The frontier molecular orbits of **COPhCN**.

Table S1. Sum of electronic and thermal Free Energies.

Fragment	Anion	Neutral
CO	-824.886145	-825.072845
CN	-973.752714	-973.640943

Table S2. SCF Energies (for the total reorganization energy calculation) from the neutral or anionic part.

Filename	Anion SCF	Number	Neutral SCF	Number
CO anion from neutral	-825.091322960	3	-825.324453601	1
CO neutral from anion	-825.113523088	2	-825.280862179	4
CN anion from neutral	-973.974115782	4	-973.908797007	2
CN neutral from anion	-974.016360775	1	-973.866803945	3

Table S3. The reactant potential energy surface (λ_2) and the product potential energy surface (λ_1) and total reorganization energies of **COCN**.

Variable	Reorganization/eV	Comment
λ_2	2.335668938	Points 4-1
λ_1	1.746741635	Points 3-2
λ (Average)	2.041205286	

Table S4. The frontier molecular orbits of **COCN** in water.
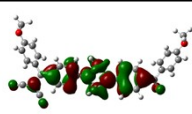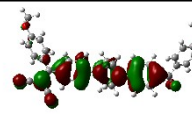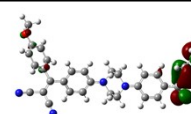
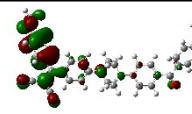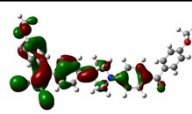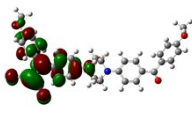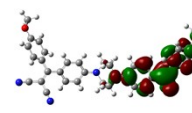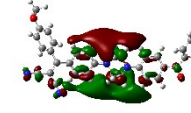| HOMO	HOMO-1	HOMO-2	HOMO-3	HOMO-9
LUMO	LUMO+1	LUMO+18		

Table S5. The singlet and triplet excited states transition configurations (%) and energy of **COCN** in water revealed by TD-DFT calculation.

	S$_1$	S$_2$	S$_3$	T$_1$	T$_2$	T$_6$
	2.6440 eV	3.4167 eV	3.8791 eV	1.7785 eV	2.6199 eV	3.6916 eV
COCN	H -> L, 80.8%	H-2 -> L, 69.0%	H-9 -> L+1, 50.3%	H -> L, 57.6%	H-2 -> L, 61.7%	H-9 -> L+1, 35.6%
	H-1 -> L, 16.1%	H-1 -> L, 24.3%	H -> L+1, 15.2%	H-1 -> L, 37.9%	H -> L, 12.8%	H-3 -> L+1, 35.1%
					H-1 -> L, 8.8%	H-3 -> L+7, 9.0%

Table S6. The calculation of **COCN** lone pair electron occupancy ratio base on Mulliken population analysis.

	S$_1$	S$_3$	T$_1$	T$_2$	T$_3$
15(N)	20.03%	0.39%	20.31%	11.06%	0.35%
16(O)	0.03%	0.44%	0.04%	5.78%	0.08%
20(N)	4.36%	2.27%	0.94%	3.75%	0.67%
31(O)	0.28%	61.95%	0.01%	0.22%	23.70%
37(O)	0.01%	-0.02%	0.00%	0.28%	11.34%
40(N)	2.85%	0.08%	6.34%	4.93%	0.11%
42(N)	2.94%	0.10%	6.57%	4.59%	0.12%
SUM	30.50%	65.21%	34.21%	30.61%	36.37%

Table S7. The singlet and triplet excited states energy of **COCO** and **CNCN** in water revealed by TD-DFT calculation.

	S$_1$	S$_2$	T$_1$	T$_2$	T$_3$	ΔE_{S1-T2}
COCO	3.1411 eV	3.8351 eV	2.4551 eV	3.0337 eV	3.2416 eV	0.1074 eV
CNCN	2.6574 eV	3.3150 eV	2.1089 eV	2.1272 eV	2.8039 eV	0.5302 eV

Table S8. The SOC constant of **COCO** and **CNCN**.

	$S_1\|HSO\|T_1$	$S_1\|HSO\|T_2$	$S_1\|HSO\|T_3$	$S_2\|HSO\|T_1$	$S_2\|HSO\|T_2$	$S_2\|HSO\|T_3$
COCO	4.3982 cm^{-1}	2.3311 cm^{-1}	2.1778 cm^{-1}	7.2602 cm^{-1}	11.7521 cm^{-1}	3.2334 cm^{-1}
CNCN	0.1244 cm^{-1}	0.1459 cm^{-1}	0.1170 cm^{-1}	0.18 cm^{-1}	0.12 cm^{-1}	0.3339 cm^{-1}

Table S9. Photophysical properties of PSs and NPs.

	λ_{abs} (nm)[a]	λ_{em} (nm)[a]	α_{AIE} [b]	$\lambda_{abs, NPs}$ (nm)[c]	$\lambda_{em, NPs}$ (nm)[c]	$\Phi_{soln.}$ (%)[d]	$\Phi_{NPs.}$ (%)[e]
COCO	350	500	0.1	280	460	1.94	0.43
COCN	350	585	25.3	350	565	0.47	62.8
CNCN	450	585	7.5	450	585	1.07	22.53

[a] Absorption and emission maximum of compounds in DMSO; [b] $\alpha_{AIE} = (I_{agger.}/I_{soln.})$; [c] Absorption and emission maximum of NPs in water; [d] Fluorescence quantum yield of compounds in DMSO; [e] Fluorescence quantum yield of NPs in water.
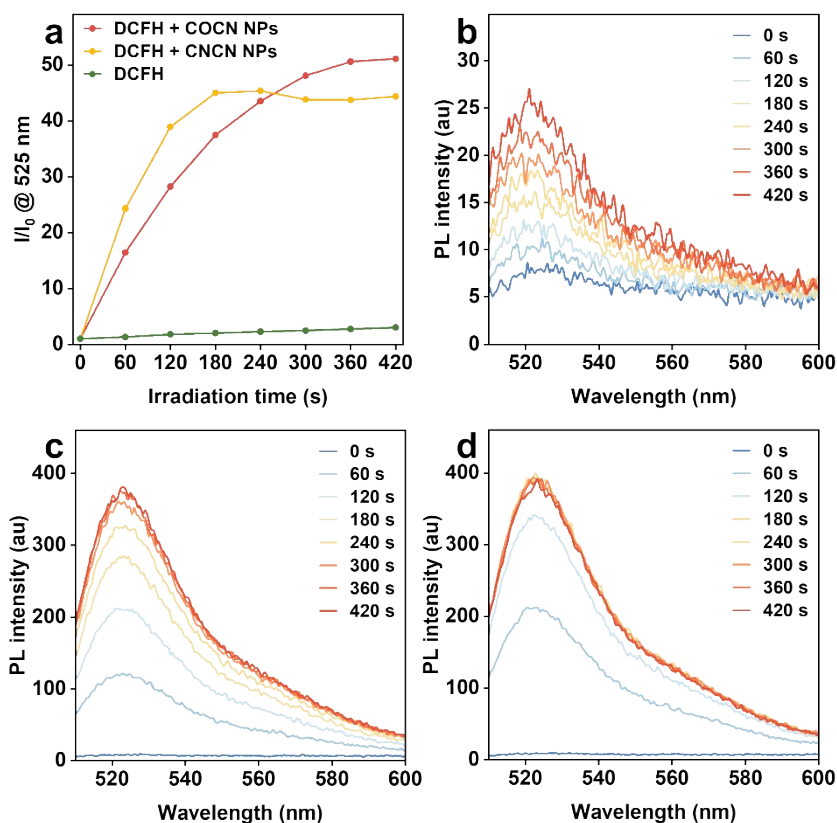

Figure S20. (a) ROS generation by **COCN NPs** and **CNCN NPs** upon white light irradiation using DCFH as an indicator. PL spectra of DCFH solutions in the presence of (b) blank, (c) **COCN NPs**, and (d) **CNCN NPs** under white light (35 mW·cm^{-2}) irradiation for different times (DCFH: 1 μM; **COCN NPs** or **CNCN NPs**: 5 μM).
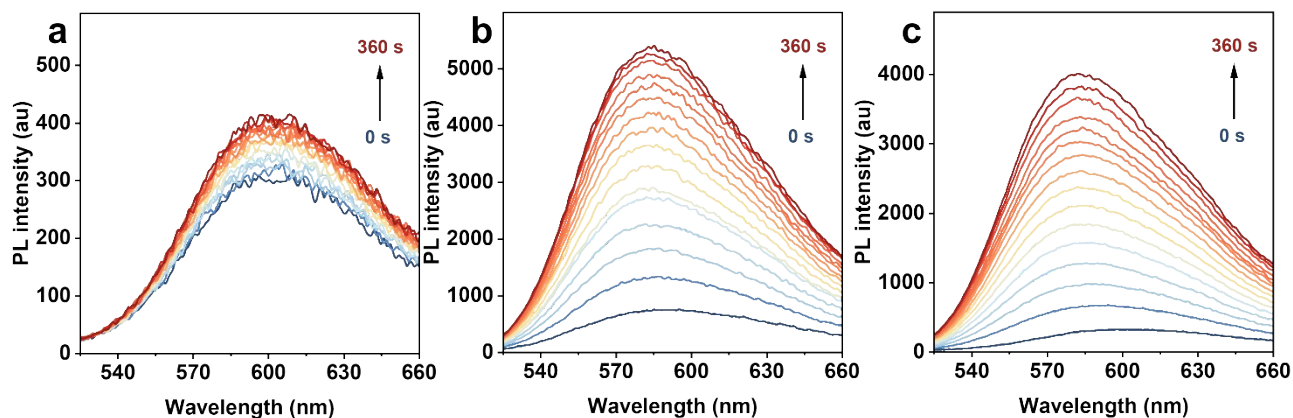
Figure S21. PL spectra of DHE solutions containing 500 μg/mL RNA in the presence of (a) blank, (b) **COCN NPs**, and (c) **CNCN NPs** with white light (35 mW·cm^{-2}) irradiation for different times (DHE: 40 μM; **COCN NPs** or **CNCN NPs**: 5 μM).
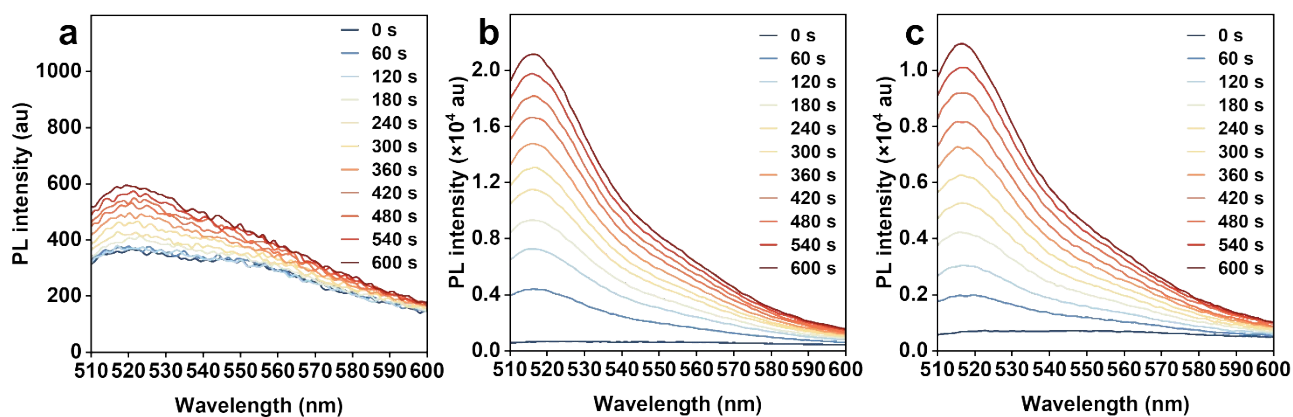

Figure S22. PL spectra of HPF solutions in the presence of (a) blank, (b) **COCN NPs**, and (c) **CNCN NPs** with white light (35 mW·cm^{-2}) irradiation for different times (HPF: 10 μM; **COCN NPs** or **CNCN NPs**: 5 μM).
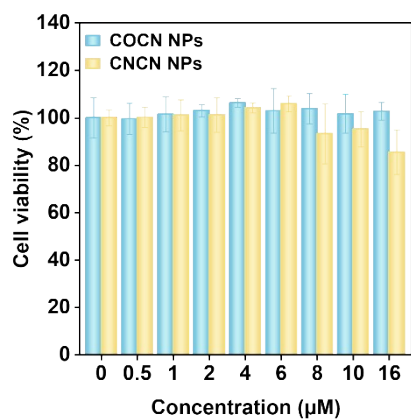
Figure S23. Cytotoxicity of **COCN NPs** and **CNCN NPs** at various concentrations (0, 0.5, 1, 2, 4, 6, 8, 10, and 16 μM) in 4T1 cells for 24 h.
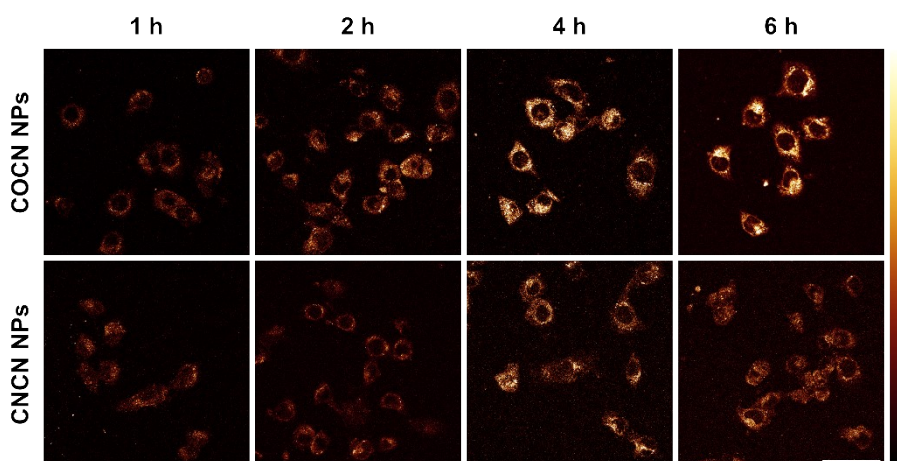

Figure S24. Evaluation of cellular uptake behaviors. CLSM images of 4T1 cells after treatment with **COCN NPs** or **CNCN NPs** (5 μM) for 1, 2, 4, or 6 h. Scale bar: 50 μm.
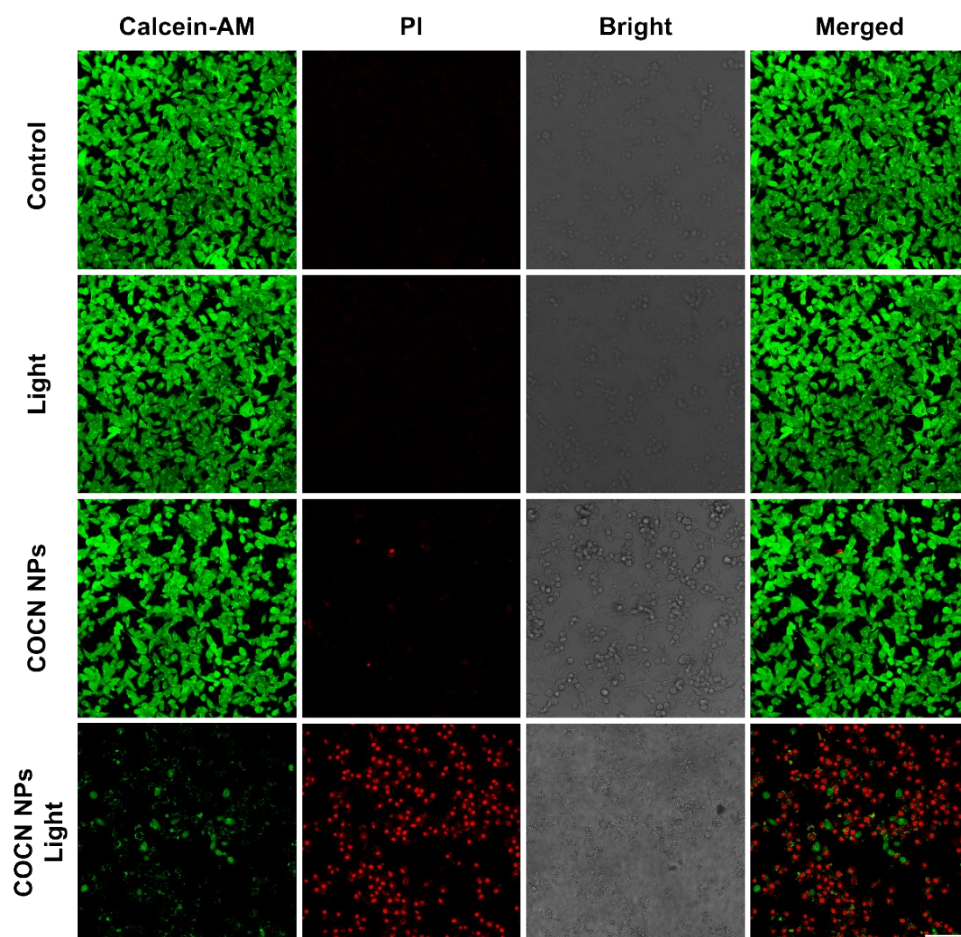
Figure S25. Live/dead staining of **COCN NPs** (8 μM) treated 4T1 cells with white light (35 mW·cm^{-2}) irradiation for 15 min under normoxic conditions. The live cells were stained by Calcein-AM (green), whereas dead cells were stained by PI (red). Scale bar: 100 μm.

Reference

1. J. E. Norton and J.-L. Brédas, Polarization Energies in Oligoacene Semiconductor Crystals, *J. Am. Chem. Soc.*, 2008, **130**, 12377-12384.

2. O. López-Estrada, H. G. Laguna, C. Barrueta-Flores and C. Amador-Bedolla, Reassessment of the Four-Point Approach to the Electron-Transfer Marcus–Hush Theory, *ACS Omega*, 2018, **3**, 2130-2140.